analytical chemistry

pubs.acs.org/ac Article

Peptide-Based Electrochemiluminescence Biosensors Using Silver Nanoclusters as Signal Probes and Pd-Cu_2O Hybrid Nanoconcaves as Coreactant Promoters for Immunoassays

Xianzhen Song,[†] Tingting Wu,[†] Chuannan Luo, Lu Zhao, Xiang Ren, Yong Zhang,* and Qin Wei*

Cite This: *Anal. Chem.* 2021, 93, 13045−13053 Read Online

ACCESS | Metrics & More | Article Recommendations | Supporting Information

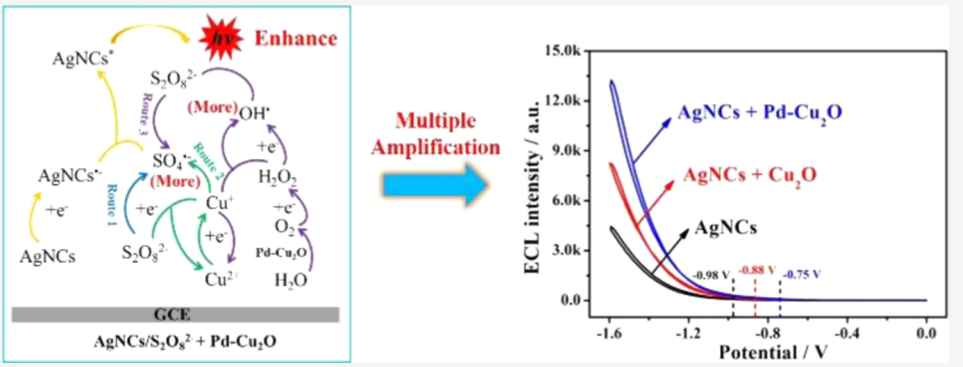

ABSTRACT: Metal nanoclusters (NCs) possess high light stability and biocompatibility because of their unique quantum size effect, which has gradually become a new type of electrochemiluminescence (ECL) nanomaterial for immunoassays. However, the luminescence efficiency of metal NCs is too low to meet the needs of trace analysis, which limits its application. Herein, Ag NCs served as signal probes and Pd-Cu_2O hybrid nanoconcaves served as coreaction promoters, developing a highly efficient peptide-based biosensor for neuron-specific enolase (NSE) detection. Utilizing the reversible cycle of Cu^+/Cu^{2+} and the reduction characteristics of Pd NPs, Pd-Cu_2O greatly accelerates the reduction of $S_2O_8^{2-}$. Meanwhile, Pd-Cu_2O has good hydrogen evolution activity, which promotes the generation of oxygen by improving the redox efficiency of the overall reaction, thus increasing the yield of active intermediates ($OH^•$) to promote the reduction of $S_2O_8^{2-}$. Specially, this is an effective attempt to use the hydrogen evolution reaction (HER) to accelerate the ECL emission of the $S_2O_8^{2-}$ system. In addition, a short peptide ligand (NARKFYKGC, NFC) was developed to implement the targeted immobilization of antibodies, which can specifically bind to the Fc fragment of antibodies, thereby avoiding the occupation of the antigen binding site (Fab fragment). The introduction of NFC not only improves the binding efficiency of antibodies but also protects its bioactivity, thus significantly improving the sensitivity of the biosensor. Based on these strategies, the proposed biosensor provides a new perspective for the applications of metal NCs in ECL systems.

Electrochemiluminescence (ECL) is a process in which the luminescent substances generate active intermediates through the gain and loss of electrons, then generate an excited state through a series of reactions, and finally convert back to the ground state with luminescence.[1−3] At present, ECL is widely used in bioanalysis, environmental monitoring, food detection, and other fields because of its excellent sensitivity and stability.[4−6] Neuron-specific enolase (NSE), an enolase existing in nervous and neuroendocrine tissues, is overexpressed in the serum of patients with small cell lung cancer (SCLC), which is important for early diagnosis and prognosis evaluation of SCLC.[7,8] Hence, there is an urgent need to develop a high-efficiency biosensor combined with ECL analysis technology to realize the sensitive detection of NSE.

Metal nanoclusters (NCs), whose size is close to the Fermi wavelength, have been widely used in the field of optical imaging and biochemical sensing due to its excellent properties such as controllable emission range, high light stability, and good water solubility and biocompatibility.[9−13] Herein, we utilized bovine serum albumin (BSA) as the template to prepare Ag NCs, which have stable cathode emission in $S_2O_8^{2-}$ solution. However, the low luminescence intensity of metal NCs restricts their application, so it is necessary to develop a highly efficient way to improve their luminescence efficiency. At present, in addition to the traditional means of acting on luminescent materials to

Received: July 16, 2021
Published: September 15, 2021

Scheme 1. Schematic Diagram for the Preparation of Ag NCs-NFC-Ab$_2$ Signal Probes and Construction Procedure of the Biosensor

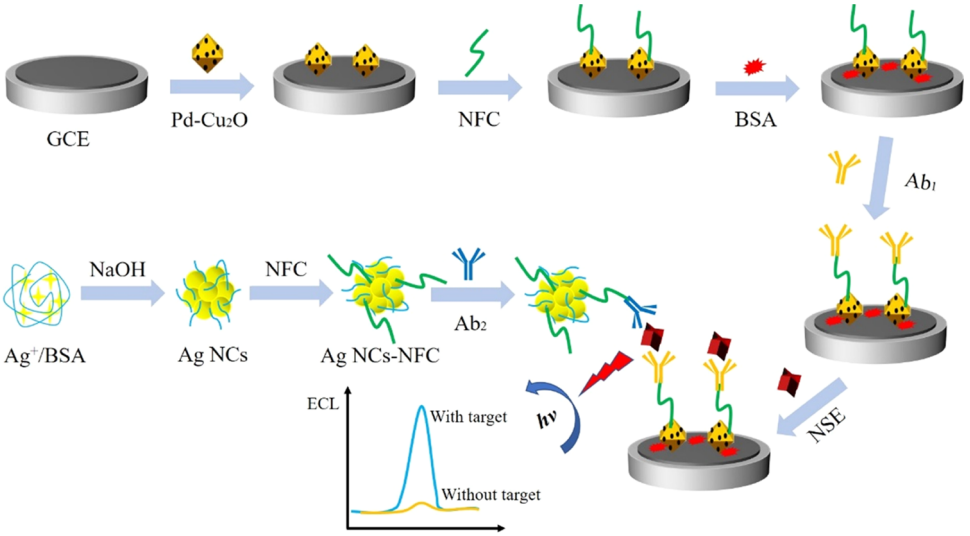

increase ECL emission, for example, developing high-performance luminophore and using the energy resonance transfer strategy, we can also focus on the catalysis of coreactants by developing high-efficiency coreaction promoters.[14−16] Therefore, a ternary reaction system including a luminophore, coreactant, and coreaction promoter was developed. The proposed ternary reaction system avoids the restrictions on the high-concentration luminophore and coreactant, which is conducive to maintaining the activity of biomarkers.[17] Herein, we developed Pd-Cu_2O hybrid nanoconcaves as coreaction promoters to realize the synergistic and efficient catalysis of coreactants. The unique nanoconcave structure of Pd-Cu_2O greatly enhances its electrocatalytic activity and stability, hence providing direction for improving the luminescence efficiency of metal NCs.

The sensitivity and stability of the biosensor are affected by the antigen recognition ability, and the binding efficiency of antigens depends on the bioactivity of the antibodies.[18] As a kind of immunoglobulin, the antigen binding sites are mainly distributed in the variable region of antibodies (Fab fragment).[19] However, the traditional method of antibody fixation is random, which is difficult to avoid the occupation of the Fab fragment, thereby affecting the bioactivity of antibodies. Therefore, it is of great significance to develop appropriate antibody affinity ligands to realize the immobilization of antibodies.[20] The short peptide ligands are composed of a few key amino acid residues and possess strong affinity with the target proteins. As the affinity ligand of antibodies, it can specifically bind to the Fc fragment, which does not participate in antigen binding and thus the bioactivity of antibodies is protected.[21] Especially, NARKFYKG octapeptide has been proved to possess high binding affinity with the 275−284 sequence in the Fc fragment of antibodies,[22] which has good physicochemical stability, low immunogenicity, convenient preparation, and low cost, exhibiting great application prospects in immunoassays.

With the above in mind, we utilized Ag NCs as signal probes, Pd-Cu_2O hybrid nanoconcaves as coreaction promoters, and the C-segment-modified NARKFYKG octapeptide by cysteine (NARKFYKGC, NFC) as a difunctional antibody orientation fixative to construct the peptide-based biosensor with high performance and activity to achieve ultrasensitive detection of NSE. Concretely, Ag NCs synthesized with BSA as the template have stable ECL emission in $S_2O_8^{2-}$ solution, which possess many fascinating characteristics, such as low toxicity, easy labeling, and excellent biocompatibility.[23,24] For the synergistic multieffect catalytic strategies, Cu^+ could catalyze the reduction of $S_2O_8^{2-}$ through redox reactions, and the oxidation product Cu^{2+} obtained electrons to regenerate Cu^+. Therefore, a large amount of sulfate radicals ($SO_4^{\bullet-}$) were generated through the reversible cycle of Cu^+/Cu^{2+}. Meanwhile, Cu_2O also has good hydrogen evolution ability, accelerating the proton transmission rate of the entire electrolytic cell system, thereby increasing the oxidation reaction efficiency and promoting the generation of O_2.[25] Subsequently, the obtained O_2 could generate reactive intermediates ($OH^{\bullet}$) through a series of reactions, which further promoted the reduction of $S_2O_8^{2-}$. By nucleating on the Cu_2O cavity and acting synergistically with it, Pd NPs not only enhance its reducibility but also improve its hydrogen evolution characteristics, thereby improving the catalytic activity in a variety of ways.[26] In addition, NFC was introduced as the bifunctional antibody fixative, which not only protected the bioactivity of the antibodies but also improved its incubation efficiency. Especially, this strategy provided the direction for improving the sensitivity of the biosensor. The proposed peptide-based biosensor realized the sensitive detection of NSE, which was of great significance for the early SCLC diagnosis. This work has opened up a new perspective for the application of metal NCs as luminophores in ECL systems and construction of the highly sensitive and active biosensors.

EXPERIMENTAL SECTION

Preparation of Cu_2O Seeds. The synthesis of Cu_2O octahedron was according to the previous method with a minor modification.[27] In brief, 0.1 mL of $CuCl_2$ (0.1 M) and 0.087 g of sodium dodecyl sulfate (SDS) were successively dispersed in 9.05 mL of ultrapure water and stirred for 10 min. After the reaction, 200 μL of NaOH (1 M) and 650 μL of $NH_2OH{\cdot}HCl$ (0.2 M) solution were added to the above solution and stirred sequentially for 30 s. Next, the resulting mixture was allowed to stand at room temperature for 3 h. Finally, the Cu_2O seeds were obtained by centrifuging (8000 rpm) and washing with ethanol three times.

https://doi.org/10.1021/acs.analchem.1c03002
Anal. Chem. 2021, 93, 13045−13053

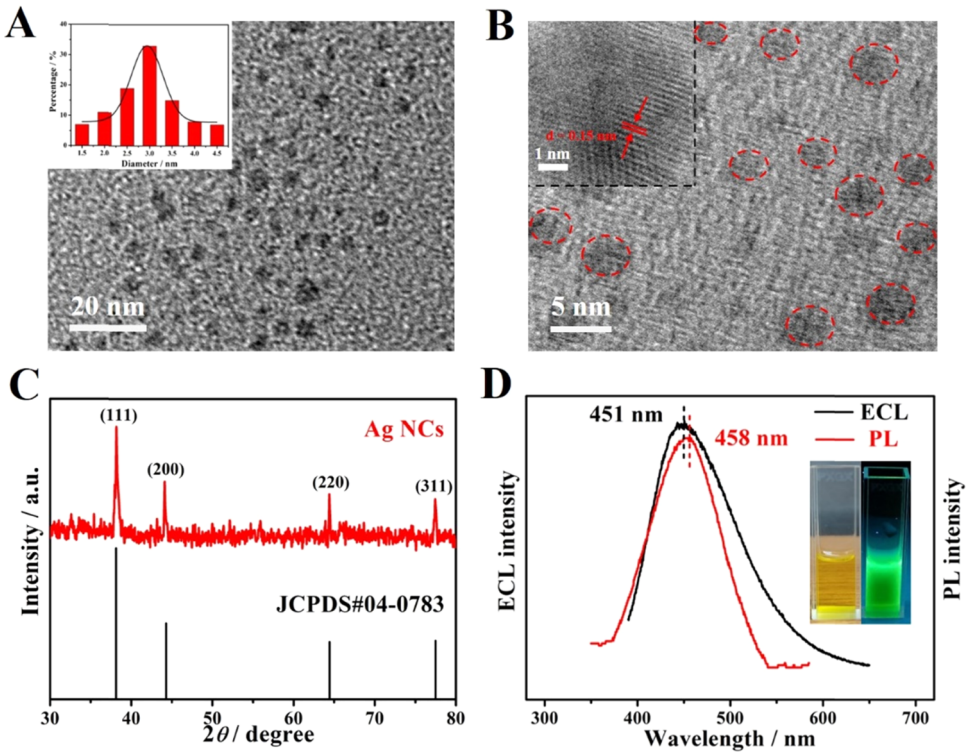

Figure 1. (A) TEM image of Ag NCs (inset: size distribution of Ag NCs). (B) HRTEM image of Ag NCs (inset: lattice fringe analysis). (C) XRD patterns and standard spectrum diagram of Ag NCs. (D) ECL and PL emission spectra of Ag NCs (inset: photographs of Ag NC solution taken with or without UV light).

Preparation of Pd-Cu_2O Hybrid Nanoconcaves. Pd-Cu_2O hybrid nanoconcaves were synthesized by the seed-based strategy.[28] Specifically, 12 mg of $Pd(acac)_2$ was dispersed in the mixed solution of 5 mL of octadecene and 1 mL of oleylamine, and 60 mg of the prepared Cu_2O seed was dissolved in 2 mL of hexane. Then, the above solution was mixed and heated at 90 °C for 15 min to evaporate hexane. After evaporation, the mixture continued to react at 120 °C for 24 h. Finally, the obtained solution was centrifuged (9500 rpm) and washed with ethanol three times.

Preparation of Ag NCs-NFC-Ab_2 Signal Probes. First, 1 mL of $AgNO_3$ (10 mM) was dispersed in 2 mL of BSA (3%). After stirring for 5 min, 200 μL of NaOH (1 M) was added and reacted at 37 °C for 12 h. Then, the resulting bright yellow solution was dialyzed for 48 h to obtain purified Ag NCs. Next, 1 mL of NFC (50 ng/mL) was put into 3 mL of the prepared Ag NCs and incubated at 4 °C for 40 min with shaking, thereby obtaining Ag NCs-NFC via Ag−S bonding. Afterward, 100 μL of Ab_2 was added to 1 mL of Ag NCs-NFC solution (dissolved in phosphate-buffered saline (PBS), pH = 7.4) and incubated at 4 °C for 1 h. Finally, 10 μL of BSA (1%) was added to the above solution and incubated for 2 h to block the inactive sites, and the obtained Ag NCs-NFC-Ab_2 signal probes were stored at 4 °C for later use.

Fabrication of the Biosensor. First, the glass carbon electrode (GCE) was polished with alumina powder to obtain a mirror-like surface and then the processed electrode was modified with 1 μL of Pd-Cu_2O (1 mg/mL). Afterward, 6 μL of NFC (50 ng/mL), 10 μL of Ab_1 (5 μg/mL), and 3 μL of BSA (1%) were dropped onto the modified electrode surface in sequence and severally incubated at 4 °C for 1 h. Next, 8 μL of NSE with different concentrations was dropped onto the electrodes and incubated at 4 °C for 40 min. Finally, 10 μL of the prepared Ag NCs-NFC-Ab_2 was dropped onto the modified electrode, and the biosensor was successfully fabricated. More importantly, the electrode should be gently rinsed with ultrapure water to remove unbound reagents after each modification step. The detailed construction process is shown in Scheme 1.

Measurement Procedure. ECL signals were tested in a three-electrode system including the reference electrode, counter electrode, and working electrode with the MPI-F flow injection chemiluminescence detector. The electrolyte is 10 mL of PBS solution containing 80 mM $S_2O_8^{2-}$ (pH = 7.4). The parameters were as follows: the voltage scan range was −1.6 to 0 V, the photomultiplier tube voltage was set to 600 V, and the scan rate was set to 0.1 V/s.

RESULTS AND DISCUSSION

Characterization Studies of Ag NCs. In Figure 1A, the particle size of the prepared Ag NCs was mainly normally distributed between 1.5 and 4.5 nm (inset) with good dispersion. To further investigate the microstructure of Ag NCs, high-resolution transmission electron microscopy (HRTEM) was utilized to characterize its lattice structure. The two-dimensional (2D) lattice fringes with a spacing of about 0.15 nm, which are consistent with the (220) lattice plane of Ag NCs (Figure 1B), are clearly observed.[29] As shown in Figure 1C, there were four distinct characteristic peaks at 38.12, 44.28, 64.40, and 77.48° in the X-ray diffraction (XRD) pattern, which were indexed to the (111), (200), (220), and (311) crystal planes of Ag NCs, respectively (JCPDS 04-0783).[30] The ECL and fluorescence (FL) emission spectra of Ag NCs are displayed in Figure 1D, a clear ECL peak was observed at 451 nm (black curve), which was close to the position of the FL emission peak (458 nm, red curve), and the bright yellow Ag NC solution (inset, left) presented green luminescence under

https://doi.org/10.1021/acs.analchem.1c03002
Anal. Chem. 2021, 93, 13045−13053

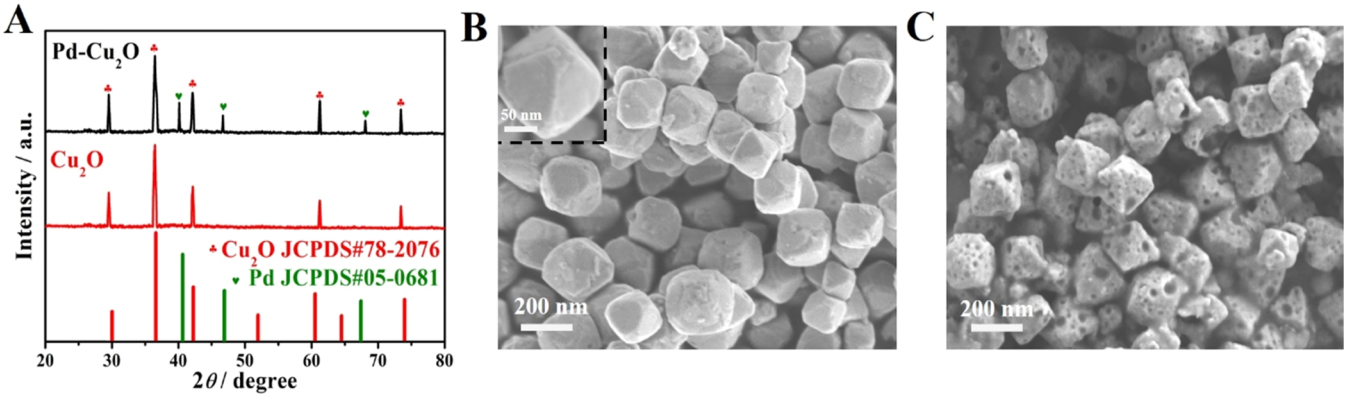

Figure 2. (A) XRD patterns of synthesized Cu_2O and Pd-Cu_2O. SEM images of (B) Cu_2O seeds and (C) Pd-Cu_2O hybrid nanoconcaves.

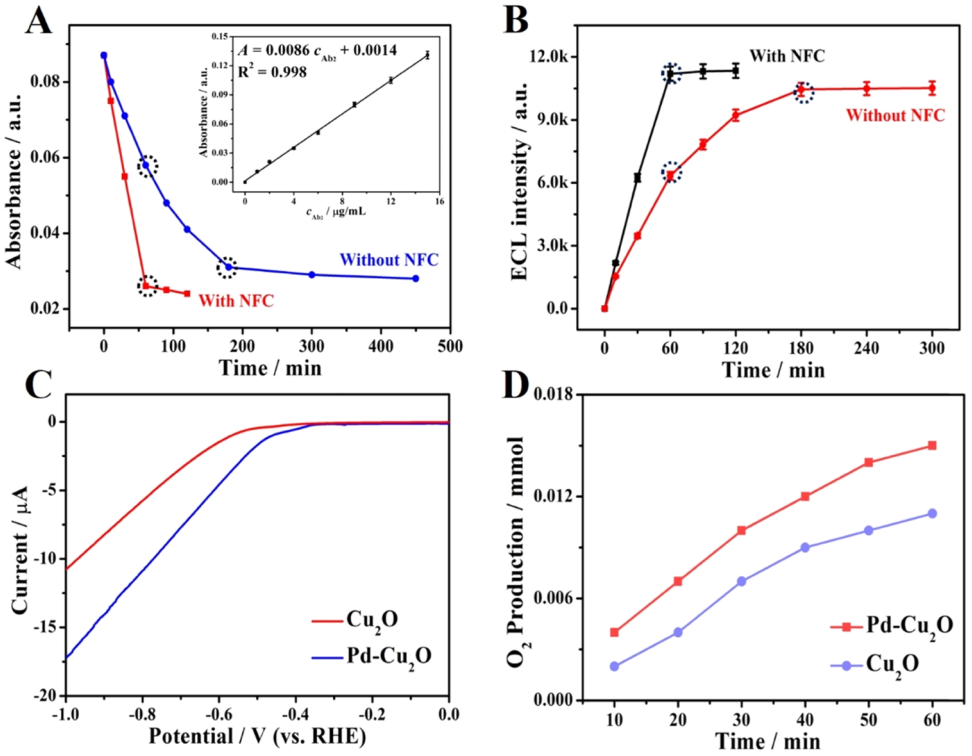

Figure 3. (A) UV−vis absorption spectra of unbound Ab_2 during the construction of the biosensor with (red curve) or without NFC (blue curve), inset: calibration curve of UV−vis absorption intensity against antibody concentration. (B) ECL responses of the biosensor with or without NFC at different incubation times of antibodies. (C) Linear sweep voltammetry (LSV) plots of Cu_2O/GCE and Pd-Cu_2O/GCE. (D) Oxygen production test in a three-electrode system catalyzed by pure Cu_2O and Pd-Cu_2O.

ultraviolet irradiation (inset, right). The above results confirmed the successful preparation of Ag NCs with good luminescence properties.

Characterization Studies of Pd-Cu_2O Hybrid Nanoconcaves. Figure 2A shows the XRD patterns for the synthesized Cu_2O and Pd-Cu_2O. The diffraction peaks at 29.6, 36.4, 42.3, 61.4, and 75.5° could be indexed to the (110), (111), (200), (220), and (310) crystal planes of Cu_2O phase, respectively (JCPDS 78-2076). Furthermore, the other diffraction peaks at 40.1, 46.7, and 68.1° matched with the simulated diagram of Pd NPs (JCPDS 05-0681), which represented the (111), (200), and (220) crystal planes.[28] As shown in Figure 2B, the Cu_2O seed presented a smooth octahedral structure with an edge length of about 150 nm. After Pd NPs were hybridized on it, the surface of Cu_2O seed was etched and the prepared Pd-Cu_2O exhibits a unique concave structure (Figure 2C, EDX spectrum and mapping images are displayed in Figure S1). Figure S2A shows the full survey XPS spectrum of Pd-Cu_2O, proving the presence of Cu, O, and Pd elements. In Figure S2B, The Cu 2p spectrum could be divided into two peaks, which were attributable to $2p_{3/2}$ (932.5 eV) and $2p_{1/2}$ (952.8 eV) of Cu^+. Meanwhile, the Pd 3d peaks at 340.8 and 335.5 eV were assigned to $3d_{3/2}$ and $3d_{5/2}$, respectively (Figure S2C). These results proved the successful preparation of Pd-Cu_2O hybrid nanoconcaves.

Research on Incubation Efficiency of Antibodies. To verify that the incubation efficiency of antibodies was improved with the addition of NFC, the ultraviolet−visible (UV−vis) absorption spectra of uncombined antibodies were acquired in the incubation environment with and without NFC. The prepared Ag NCs and Ag NCs-NFC were both incubated with 1 mL of 10 μg/mL Ab_2 at 4 °C, and the supernatant containing

https://doi.org/10.1021/acs.analchem.1c03002
Anal. Chem. 2021, 93, 13045−13053

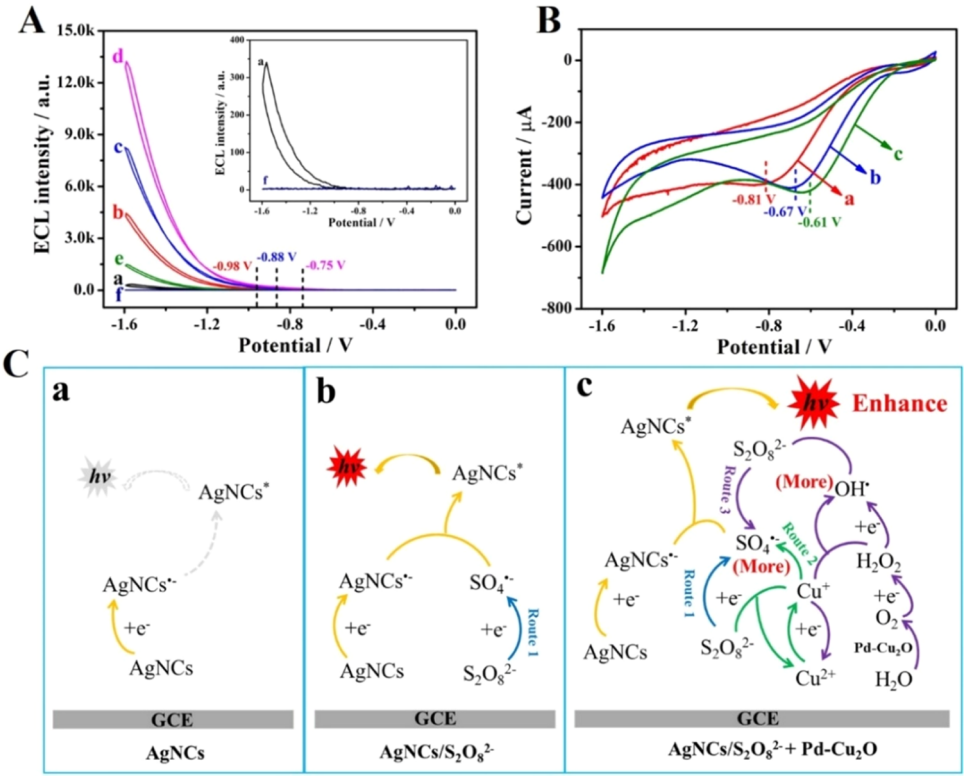

Figure 4. (A) ECL−potential curves of (a) GCE, (b) GCE/Ag NCs, (c) GCE/Ag NCs/Cu_2O, (d) GCE/Ag NCs/Pd-Cu_2O, (e) GCE/Pd-Cu_2O-modified electrodes in PBS containing 80 mM $S_2O_8^{2-}$, and (f) GCE/Ag NCs/Pd-Cu_2O-modified electrodes in pure PBS. (B) CV responses of (a) GCE/Ag NCs, (b) GCE/Ag NCs/Cu_2O, and (c) GCE/Ag NCs/Pd-Cu_2O-modified electrodes in PBS containing 80 mM $S_2O_8^{2-}$. (C) Possible ECL mechanism for (a) Ag NCs, (b) Ag NCs/$S_2O_8^{2-}$, and (c) Ag NCs/$S_2O_8^{2-}$ + Pd-Cu_2O systems.

uncombined Ab_2 was collected with different incubation times. Finally, the collected supernatant was subjected to UV−vis analysis. As shown in Figure 3A, the UV−vis absorption intensity of the supernatant collected from the Ag NCs-NFC-Ab_2 system stabilized within about 1 h (red curve), while the UV−vis absorption intensity of the supernatant collected from Ag NCs-Ab_2 tended to be stable after 3 h of incubation (blue curve). In addition, the number of bound antibodies of Ag NCs-NFC-Ab_2 was calculated to be 7.14 μg by the calibration equation (A = 0.0090c + 0.0021, A: absorbance, c: Ab_2 concentration) at 1 h, while the number of binding antibodies of Ag NCs-Ab_2 was 3.42 μg after the same time. Hence, the results confirmed that NFC could significantly enhance the incubation efficiency of antibodies.

Subsequently, we tested the ECL responses of the proposed biosensor with or without NFC at different antibody incubation times to further demonstrate the above results. In Figure 3B, the ECL response of the biosensor with NFC attained maximum in about 1 h (black curve), and the biosensor without NFC revealed the highest ECL signal in 3 h (red curve), suggesting that 1 h was the ideal incubation time. Simultaneously, the optimal ECL signal of the biosensor with NFC was better than that without NFC involvement, which may be attributed to the directional fixation of antibodies.

Enhanced ECL Emissions Based on the HER Effect. First, we tested the linear sweep voltammetry (LSV) responses of pure Cu_2O and Pd-Cu_2O to explore their hydrogen evolution ability. As shown in Figure 3C, Pd-Cu_2O showed a lower potential of −548 mV than the pure Cu_2O (−681 mV) to drive the same current of −3 μA, suggesting that Pd-Cu_2O hybrid nanoconcaves possessed better HER performance. Afterward, the efficient HER process initiated by Pd-Cu_2O promoted the proton transfer rate of the whole electrolyte environment. Hence, the efficiency of the anodic oxidation reaction was also improved to keep the balance of the electrolysis system, which makes the water to be oxidized into more O_2, thus providing more radicals for ECL emission.[31]

To further verify that HER could promote the generation of O_2, an H-type electrolytic cell with a tube was designed to calculate the amount of oxygen evolution. In the H-type electrolytic cell, the working electrode (proposed biosensor) and reference electrode (Ag/AgCl) were in the same reaction chamber, and the counter electrode (Pt electrode) was solely in another reaction chamber (Figure S5). In the voltage range of 0 to −1 V, bubbles could be observed at the working electrode, indicating the occurrence of HER. Meanwhile, a lot of bubbles appeared at the Pt electrode surface of the anode, indicating the generation of O_2. The measurements of chronoamperometry were carried out under the voltage of −600 mV applied to the working electrode, and the released O_2 was calculated by the amount of electrolyte discharged from the anode chamber. In Figure 3D, it could be observed that the O_2 production in the anode chamber of Cu_2O and Pd-Cu_2O increased gradually with the extension of reaction time. Meanwhile, the O_2 production obtained with Pd-Cu_2O was close to 1.5 times that of the pure Cu_2O, indicating that the improvement of HER by Pd-Cu_2O could indeed promote the enhancment of O_2 production. Afterward, a mass of reactive intermediates ($OH^•$) was generated to react with $S_2O_8^{2-}$ to obtain more $SO_4^{•-}$, thereby greatly enhancing the luminescence efficiency of the metal NCs.

Discussion on Multiple Signal Amplification Mechanism. In this study, the ECL responses of bare GCE, Ag NCs/

https://doi.org/10.1021/acs.analchem.1c03002
Anal. Chem. 2021, 93, 13045−13053

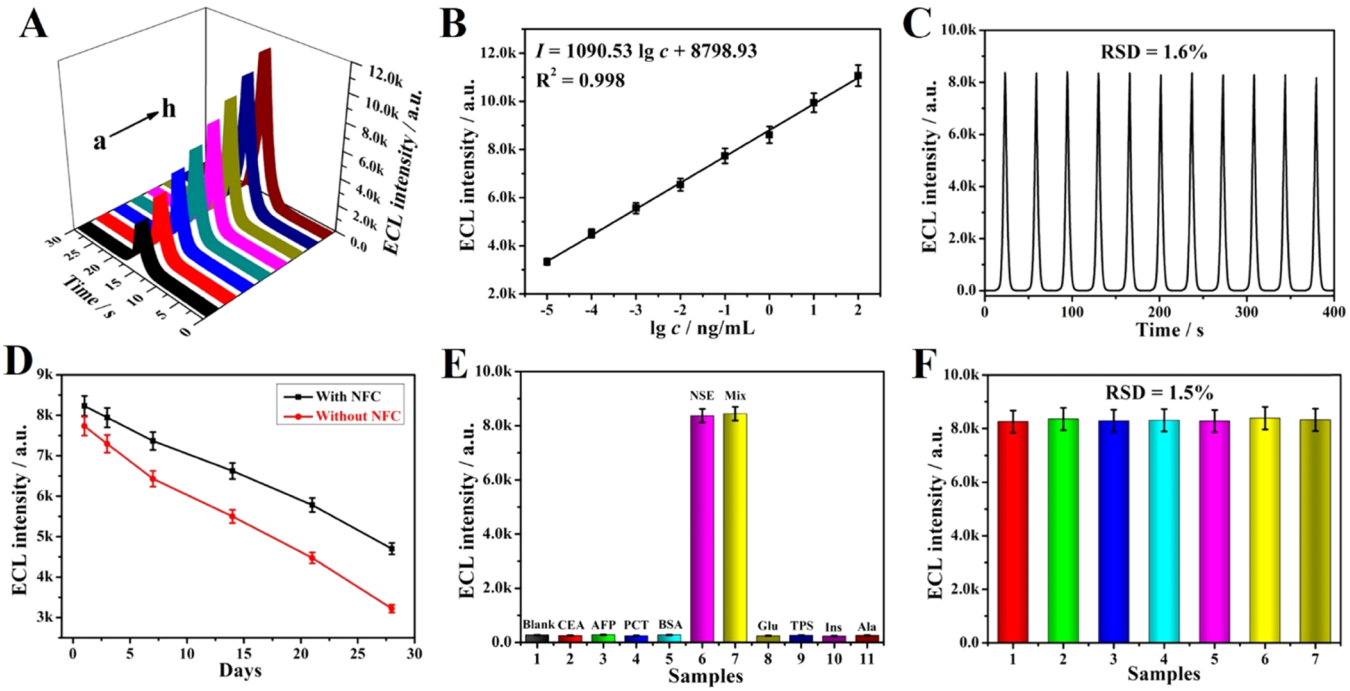

Figure 5. (A) ECL responses with different concentrations of NSE (a−h: 10 fg/mL, 100 fg/mL, 1 pg/mL, 10 pg/mL, 100 pg/mL, 1 ng/mL, 10 ng/mL, and 100 ng/mL). (B) Corresponding calibration curve for NSE detection. (C) Operation and (D) storage stability, (E) selectivity, and (F) reproducibility of the proposed biosensor.

GCE, Ag NCs/Cu_2O/GCE, Ag NCs/Pd-Cu_2O/GCE, and Pd-Cu_2O/GCE were measured in PBS containing 80 mM $S_2O_8^{2-}$, and the ECL response of Ag NCs/Pd-Cu_2O/GCE was tested in pure PBS. As shown in Figure 4A, the bare GCE (curve a) showed a low ECL emission in $S_2O_8^{2-}$ solution. After modifying with Ag NCs (curve b), there was an obvious ECL signal of about 4500 au, which was due to the stable cathode emission of Ag NCs in $S_2O_8^{2-}$. Afterward, the enhanced ECL signal of about 8000 au was obtained with further modification of Cu_2O (curve c), which indicated that Cu_2O could promote the luminescence of the Ag NCs/$S_2O_8^{2-}$ system. When Ag NCs/Pd-Cu_2O was modified on the electrode surface, the proposed biosensor showed extremely high ECL response, which was approximately three times that of pure Ag NCs (curve d). At the same time, Ag NCs/Pd-Cu_2O/GCE had almost no ECL emission in PBS (curve f). Therefore, we could infer that the prepared Pd-Cu_2O hybrid nanoconcaves had higher catalytic performance for $S_2O_8^{2-}$, which enhanced the ECL signal by promoting the reduction of the coreactant, rather than acting on the luminophore. Interestingly, Pd-Cu_2O/GCE exhibited an enhanced ECL signal than that of bare GCE in $S_2O_8^{2-}$ (curve e), which further demonstrated the above amplification mechanism.

In addition, we tested the CV responses of Ag NCs/GCE, Ag NCs/Cu_2O/GCE, and Ag NCs/Pd-Cu_2O/GCE-modified electrodes in $S_2O_8^{2-}$. In Figure 4B, the reduction peak potential of Ag NCs/Pd-Cu_2O was −0.61 V, while the reduction peak potentials of Ag NCs and Ag NCs/Cu_2O were −0.67 and −0.81 V, respectively, and the corresponding peak currents increased sequentially. The results confirmed that Pd-Cu_2O greatly promoted the reduction of $S_2O_8^{2-}$ and increased the electron transfer rate of the overall reaction. Meanwhile, the above results were consistent with the initial potential change trend of ECL emission in Figure 4A (−0.98 to −0.75 V), confirming the enhancement of the ECL response of Pd-Cu_2O to Ag NCs. Therefore, the introduction of Pd-Cu_2O can improve the luminescence efficiency and realize the strong luminescence of Ag NCs at low potential.

Possible ECL Mechanism. Figure 4C shows the possible ECL reaction process. Specifically, Ag NCs had no ECL emission in the absence of coreactants (Figure 4C,a). When $S_2O_8^{2-}$ was added to PBS, a small amount of $SO_4^{\bullet-}$ was generated on the electrode surface, and then reacted with Ag $NCs^{\bullet-}$ to obtain a weaker ECL emission (Figure 4C,b). After the modification of Pd-Cu_2O, a great deal of $SO_4^{\bullet-}$ was obtained through its catalysis in various ways, thereby greatly amplifying the ECL signal (Figure 4C,c). The detailed reaction mechanism was as follows: In route 1, a small amount of $SO_4^{\bullet-}$ was produced by gaining electrons on the electrode surface to obtain a weaker ECL emission (eq 1). In route 2, $S_2O_8^{2-}$ was reduced by Cu^+ to generate more $SO_4^{\bullet-}$, and Cu^{2+} as the accompanying product could obtain electrons on the electrode surface to regenerate Cu^+, thereby continuously generating $SO_4^{\bullet-}$ through the reversible redox reaction of Cu^+/Cu^{2+} (eqs 2 and 3). In route 3, the overall oxidation−reduction reaction efficiency was improved due to the good HER performance of Pd-Cu_2O, thereby promoting the generation of O_2. Subsequently, the obtained O_2 could generate a large amount of $OH^{\bullet}$ through a series of reactions, which reacted with $S_2O_8^{2-}$ to form $SO_4^{\bullet-}$ (eqs 4−8). During the ECL emission process, Ag NCs first obtained electrons to generate Ag $NCs^{\bullet-}$, then reacted with $SO_4^{\bullet-}$ to obtain the excited-state species (Ag NCs*), and finally produced strong ECL emission (eqs 9−11).

Route 1:

$$S_2O_8^{2-} + e^- \rightarrow SO_4^{2-} + SO_4^{\bullet-} \quad (1)$$

Route 2:

$$Cu^+ + S_2O_8^{2-} \rightarrow Cu^{2+} + SO_4^{2-} + SO_4^{\bullet-} \quad (2)$$

https://doi.org/10.1021/acs.analchem.1c03002
Anal. Chem. 2021, 93, 13045−13053

$$Cu^{2+} + e^- \rightarrow Cu^+ \quad (3)$$

Route 3:

$$2H_2O \rightarrow 4H^+ + 4e^- + O_2 \quad (4)$$

$$O_2 + 2H_2O + 2e^- \rightarrow 2OH^- + H_2O_2 \quad (5)$$

$$H_2O_2 + e^- \rightarrow OH^- + OH^\bullet \quad (6)$$

or

$$Cu^+ + H_2O_2 \rightarrow Cu^{2+} + OH^- + OH^\bullet(\text{more}) \quad (7)$$

$$OH^\bullet + S_2O_8^{2-} \rightarrow O_2 + HSO_4^- + SO_4^{\bullet-}(\text{more}) \quad (8)$$

ECL emission:

$$Ag\,NCs + e^- \rightarrow Ag\,NCs^{\bullet-} \quad (9)$$

$$Ag\,NCs^{\bullet-} + SO_4^{\bullet-} \rightarrow Ag\,NCs^* + SO_4^{2-} \quad (10)$$

$$Ag\,NCs^* \rightarrow Ag\,NCs + h\nu \quad (11)$$

ECL Performances of the Proposed Biosensor. Sensitive and efficient detectability of the ECL biosensor for NSE is confirmed by ECL intensity−time curves (Figure 5A) and the corresponding calibration curve (Figure 5B) under the optimized environment. The results showed a good linear correlation between ECL intensity and antigen concentration (I = 1090.53 lg$c$ + 8798.93, I: ECL intensity, c: antigen concentration) with the correlation coefficient of 0.998. Compared with the previous reported works (Table S1), the proposed ECL biosensor was sensitive in a wide range of 10 fg/mL and 100 ng/mL with the low detection limit calculated at 3.65 fg/mL (S/N = 3) for NSE analysis.

Stability, Selectivity, and Reproducibility of the Proposed Biosensor. The ECL test under 11 cycles of electrode scanning was utilized for verifying the stability of the proposed biosensor. In Figure 5C, the biosensor could maintain stable signal strength in multiple cycles, and the relative standard deviation (RSD) was 1.6%, which explained that the proposed biosensor owned good stability. After the NFC was introduced into the biosensor, the decreasing amplitude of the ECL signal was significantly smaller than that of the biosensor without NFC (Figure 5D). This shows that the introduction of NFC was conducive to build the long-life biosensor by protecting the activity of biomarkers. In addition, the selectivity of the biosensor was investigated by measuring the ECL responses of NSE and other interferences (Figure 5E). There was a large difference in the ECL signals between NSE and other interferences (carcinoembryonic antigen, α fetoprotein, procalcitonin, bovine serum albumin, glucose, tryptase, insulin, alanine), and the ECL responses of these interferences were close to that of the blank sample. Meanwhile, the ECL response of NSE was almost the same as that of the mixed sample (1 ng/mL NSE + 10 ng/mL interferences), indicating good selectivity of the biosensor. Finally, for reproducibility, ECL tests were carried out with seven different electrodes under the same conditions. As can be seen from Figure 5F, the measured ECL signals of these electrodes have tiny differences with the RSD of 1.5%, showing nice reproducibility of the biosensor.

Analysis of Serum Samples. To investigate the clinical practicability of the proposed biosensor, the standard addition method was utilized by adding different concentrations of NSE as the spiked samples into the initial human serum samples. After testing 11 times on each sample, the corresponding recovery and RSD were calculated to analyze the accuracy and precision of the biosensor in serum samples. As revealed in Table 1, the calculated recovery and RSD were 95.0−103 and 1.0−2.4%, respectively, suggesting the proposed biosensor possessed good accuracy and precision in serum sample analysis and fitted the bill for the clinical diagnosis of SCLC.

Table 1. Detection of NSE in Human Serum Samples

initial concentration (ng/mL)	spiked samples (ng/mL)	average found (ng/mL, n = 11)	RSD (%)	recovery (%)
0.150	0.110	0.259	2.2	99.1
	0.120	0.269	2.4	99.2
	0.130	0.281	2.1	101
1.00	0.200	1.19	1.5	95.0
	0.400	1.41	1.4	103
	0.600	1.60	1.2	100
3.00	0.500	3.48	1.3	96.0
	1.00	4.02	1.1	102
	2.00	4.94	1.0	97.0

CONCLUSIONS

In summary, we utilized Ag NCs-NFC-Ab$_2$ as the signal probes, $K_2S_2O_8$ as the coreactant, and Pd-Cu_2O as the highly efficient coreaction promoter to construct a ternary reaction system for NSE analysis. The unique size structure of Ag NCs made it have stable luminescence property, which provided prospects for its application in immunoassays. At the same time, its good water solubility and biocompatibility also provided protection for the activity of the biosensor. Pd-Cu_2O hybrid nanoconcaves had high catalytic activity, which could promote the reduction of $S_2O_8^{2-}$ through chemical catalysis and electrocatalysis, thereby generating more $SO_4^{\bullet-}$ for improving ECL emission. Based on the reversible cycle of Cu^+/Cu^{2+} and the efficient reduction of Pd NPs, as well as the excellent HER performance and high ECSA of Pd-Cu_2O, the luminescence efficiency of Ag NCs was greatly enhanced, thus improving the sensitivity of the biosensor. In addition, NFC developed as a small peptide antibody affinity ligand was introduced into the proposed biosensor, which was beneficial to the activity protection and incubation process of the antibodies, and provided a new perspective for the construction of high-activity and high-sensitivity biosensors. The proposed biosensor had excellent stability, selectivity, and reproducibility and showed good accuracy and precision in serum sample analysis, realizing sensitive detection of NSE. This work expands the application of metal NCs in ECL systems, and has certain promotion significance for the diagnosis of early lung cancer.

ASSOCIATED CONTENT

Supporting Information

The Supporting Information is available free of charge at https://pubs.acs.org/doi/10.1021/acs.analchem.1c03002.

Materials and reagents, apparatus, pretreatment of human serum samples, EDX spectrum and mapping images of Pd-Cu_2O, XPS spectra of Pd-Cu_2O, research on binding efficiency of NFC to Ag NCs, electroactive surface areas of Cu_2O and Pd-Cu_2O, schematic diagram of self-assembled electrolytic cell device, electrochemical characterization of the proposed biosensor, condition optimization, and Table S1 (PDF)

https://doi.org/10.1021/acs.analchem.1c03002
Anal. Chem. 2021, 93, 13045−13053

AUTHOR INFORMATION

Corresponding Authors

Yong Zhang − *Collaborative Innovation Center for Green Chemical Manufacturing and Accurate Detection, Key Laboratory of Interfacial Reaction & Sensing Analysis in Universities of Shandong, School of Chemistry and Chemical Engineering, University of Jinan, Jinan 250022 Shandong, China;* orcid.org/0000-0002-5831-637X; Phone: +86 531 82765730; Email: yongzhang7805@126.com; Fax: +86 531 82765969

Qin Wei − *Collaborative Innovation Center for Green Chemical Manufacturing and Accurate Detection, Key Laboratory of Interfacial Reaction & Sensing Analysis in Universities of Shandong, School of Chemistry and Chemical Engineering, University of Jinan, Jinan 250022 Shandong, China;* orcid.org/0000-0002-3034-8046; Phone: +86 531 82765730; Email: sdjndxwq@163.com; Fax: +86 531 82765969

Authors

Xianzhen Song − *Collaborative Innovation Center for Green Chemical Manufacturing and Accurate Detection, Key Laboratory of Interfacial Reaction & Sensing Analysis in Universities of Shandong, School of Chemistry and Chemical Engineering, University of Jinan, Jinan 250022 Shandong, China*

Tingting Wu − *Collaborative Innovation Center for Green Chemical Manufacturing and Accurate Detection, Key Laboratory of Interfacial Reaction & Sensing Analysis in Universities of Shandong, School of Chemistry and Chemical Engineering, University of Jinan, Jinan 250022 Shandong, China*

Chuannan Luo − *Collaborative Innovation Center for Green Chemical Manufacturing and Accurate Detection, Key Laboratory of Interfacial Reaction & Sensing Analysis in Universities of Shandong, School of Chemistry and Chemical Engineering, University of Jinan, Jinan 250022 Shandong, China*

Lu Zhao − *Collaborative Innovation Center for Green Chemical Manufacturing and Accurate Detection, Key Laboratory of Interfacial Reaction & Sensing Analysis in Universities of Shandong, School of Chemistry and Chemical Engineering, University of Jinan, Jinan 250022 Shandong, China*

Xiang Ren − *Collaborative Innovation Center for Green Chemical Manufacturing and Accurate Detection, Key Laboratory of Interfacial Reaction & Sensing Analysis in Universities of Shandong, School of Chemistry and Chemical Engineering, University of Jinan, Jinan 250022 Shandong, China;* orcid.org/0000-0002-4321-4282

Complete contact information is available at: https://pubs.acs.org/10.1021/acs.analchem.1c03002

Author Contributions

†X.S. and T.W. contributed equally.

Notes

The authors declare no competing financial interest.

ACKNOWLEDGMENTS

This study was supported by the National Key Scientific Instrument and Equipment Development Project of China (No. 21627809), the National Natural Science Foundation of China (Nos. 21777056, 21427808), the Special Foundation for Taishan Scholar Professorship of Shandong Province, the Jinan Scientific Research Leader Workshop Project (2018GXRC024, 2018GXRC021), and the Innovation Team Project of Colleges and Universities in Jinan (No. 2019GXRC027).

REFERENCES

(1) Hu, L. Z.; Xu, G. B. *Chem. Soc. Rev.* **2010**, *39*, 3275−3304.
(2) Wen, W.; Yan, X.; Zhu, C. Z.; Du, D.; Lin, Y. H. *Anal. Chem.* **2017**, *89*, 138−156.
(3) Qi, H. L.; Zhang, C. X.; Huang, Z.; Wang, L.; Wang, W. N.; Bard, A. J. *J. Am. Chem. Soc.* **2016**, *138*, 1947−1954.
(4) Dong, Y. P.; Zhou, Y.; Wang, J.; Zhu, J. J. *Anal. Chem.* **2016**, *88*, 5469−5475.
(5) Gao, W. Y.; Liu, Z. Y.; Qi, L. M.; Lai, J. P.; Kitte, S. A.; Xu, G. B. *Anal. Chem.* **2016**, *88*, 7654−7659.
(6) Deiss, F.; LaFratta, C. N.; Symer, M.; Blicharz, T. M.; Sojic, N.; Walt, D. R. *J. Am. Chem. Soc.* **2009**, *131*, 6088−6089.
(7) Dharandas, R. S. A.; Gustavo, J.; Eduardo, F.; Gala, C.; Guillem, C.; Marco, H. E.; Paula, S. S.; Xavier, F.; Monica, M.; Manel, S. *J. Am. Coll. Cardiol.* **2017**, *69*, No. 166.
(8) Simona, F.; Federica, B.; Roberto, L.; Monica, T.; Simone, C.; Mauro, P. *Clin. Chem.* **2020**, *66*, 667−675.
(9) Hesari, M.; Workentin, M. S.; Ding, Z. *Chem. Sci.* **2014**, *5*, 3814−3822.
(10) Hesari, M.; Workentin, M. S.; Ding, Z. *ACS Nano* **2014**, *8*, 8543−8553.
(11) Chen, T. T.; Hu, Y. H.; Cen, Y.; Chu, X.; Lu, Y. *J. Am. Chem. Soc.* **2013**, *135*, 11595−11602.
(12) Xiao, F. X.; Zeng, Z. P.; Liu, B. *J. Am. Chem. Soc.* **2015**, *137*, 10735−10744.
(13) Sementa, L.; Barcaro, G.; Dass, A.; Stener, M.; Fortunelli, A. *Chem. Commun.* **2015**, *51*, 7935−7938.
(14) Song, X. Z.; Li, X. J.; Wei, D.; Feng, R.; Yan, T.; Wang, Y. G.; Ren, X.; Du, B.; Ma, H. M.; Wei, Q. *Biosens. Bioelectron.* **2019**, *126*, 222−229.
(15) Zhao, L.; Song, X. Z.; Ren, X.; Fan, D. W.; Wei, Q.; Wu, D. *Anal. Chem.* **2021**, *93*, 8613−8621.
(16) Zhao, L.; Song, X. Z.; Ren, X.; Wang, H.; Fan, D. W.; Wu, D.; Wei, Q. *Biosens. Bioelectron.* **2021**, *191*, 113409.
(17) Song, X. Z.; Shao, X. R.; Dai, L.; Fan, D. W.; Ren, X.; Sun, X.; Luo, C. N.; Wei, Q. *ACS Appl. Mater. Interfaces* **2020**, *12*, 9098−9106.
(18) Makaraviciute, A.; Ramanaviciene, A. *Biosens. Bioelectron.* **2013**, *50*, 460−471.
(19) Dostalova, S.; Cerna, T.; Hynek, D.; Koudelkova, Z.; Vaculovic, T.; Kopel, P.; Hrabeta, J.; Heger, Z.; Vaculovicova, M.; Eckschlager, T.; Stiborova, M.; Adam, V. *ACS Appl. Mater. Interfaces* **2016**, *8*, 14430−14441.
(20) Liu, F.; Wang, L.; Wang, H. W.; Yuan, L.; Li, J. W.; Brash, J. L.; Chen, H. *ACS Appl. Mater. Interfaces* **2015**, *7*, 3717−3724.
(21) Verdoliva, A.; Marasco, D.; De Capua, A.; Saporito, A.; Bellofiore, P.; Manfredi, V.; Fattorusso, R.; Pedone, C.; Ruvo, M. *ChemBioChem* **2005**, *6*, 1242−1253.
(22) Sugita, T.; Katayama, M.; Okochi, M.; Kato, R.; Ichihara, T.; Honda, H. *Biochem. Eng. J.* **2013**, *79*, 33−40.
(23) Zhou, Y.; Chen, M. X.; Zhuo, Y.; Chai, Y. Q.; Xu, W. J.; Yuan, R. *Anal. Chem.* **2017**, *89*, 6787−6793.
(24) Zhou, Y.; Wang, H. J.; Zhuo, Y.; Chai, Y. Q.; Yuan, R. *Anal. Chem.* **2017**, *89*, 3732−3738.
(25) Song, C. X.; Zhao, Z. Y.; Sun, X. X.; Zhou, Y. H.; Wang, Y.; Wang, D. B. *Small* **2019**, *15*, No. 1804268.
(26) Xiao, P.; Buijnsters, J. G.; Zhao, Y. X.; Yu, H.; Xu, X. L.; Zhu, Y. J.; Tang, D. H.; Zhu, J. J.; Zhao, Z. *J. Catal.* **2019**, *380*, 215−223.
(27) Madasu, M.; Huang, M. H. *Catal. Sci. Technol.* **2020**, *10*, 6948−6952.
(28) Li, L. L.; Chen, X. B.; Wu, Y.; Wang, D. S.; Peng, Q.; Zhou, G.; Li, Y. D. *Angew. Chem., Int. Ed.* **2013**, *52*, 11049−11053.
(29) Yu, D. B.; Yam, V. W. W. *J. Am. Chem. Soc.* **2004**, *126*, 13200−13201.

(30) Zhao, Y.; Kornienko, N.; Liu, Z.; Zhu, C.; Asahina, S.; Kuo, T.-R.; Bao, W.; Xie, C.; Hexemer, A.; Terasaki, O.; Yang, P.; Yaghi, O. M. *J. Am. Chem. Soc.* **2015**, *137*, 2199−2202.
(31) Zhao, L.; Kuang, X.; Chen, C.; Sun, X.; Wang, Z. L.; Wei, Q. *Chem. Commun.* **2019**, *55*, 10170−10173.

https://doi.org/10.1021/acs.analchem.1c03002
Anal. Chem. 2021, 93, 13045−13053